David L. S. Hung[1]
University of Michigan-Shanghai Jiao Tong University Joint Institute,
National Engineering Laboratory for Automotive Electronic Control Technology,
Shanghai Jiao Tong University,
Shanghai 200240, China
e-mail: dhung@sjtu.edu.cn

Hao Chen
National Engineering Laboratory for Automotive Electronic Control Technology,
School of Mechanical Engineering,
Shanghai Jiao Tong University,
Shanghai 200240, China
e-mail: chenhow2008@sjtu.edu.cn

Min Xu
National Engineering Laboratory for Automotive Electronic Control Technology,
School of Mechanical Engineering,
Shanghai Jiao Tong University,
Shanghai 200240, China
e-mail: mxu@sjtu.edu.cn

Jie Yang
National Engineering Laboratory for Automotive Electronic Control Technology,
School of Mechanical Engineering,
Shanghai Jiao Tong University,
Shanghai 200240, China
e-mail: yangjiejt@gmail.com

Hanyang Zhuang
University of Michigan-Shanghai Jiao Tong University Joint Institute,
Shanghai Jiao Tong University,
Shanghai 200240, China,
e-mail: zhuanghany11@sjtu.edu.cn

Experimental Investigation of the Variations of Early Flame Development in a Spark-Ignition Direct-Injection Optical Engine

Experiments under two intake air swirl levels (swirl ratios of 0.55 and 5.68) were conducted in order to investigate the early flame development of combustion in a single-cylinder spark-ignition direct-injection engine. The engine was equipped with a quartz insert in the piston, which provided an optical access to its cylinder through the piston. The crank angle resolved combustion images through the piston window and in-cylinder pressure measurements of 250 cycles were simultaneously recorded for both swirl levels at a specified engine speed and low load condition. The early development, size, and spatial characteristics extracted from the flame images were analyzed as a function of crank angle degrees after the ignition. The experimental results revealed that the early flame development was strongly influenced by the highly directed swirl motion of intake-air into the combustion cylinder. The location of the start of the flame kernel relative to the spark plug position also changed intermittently at different swirl levels. While the structure of the early flame was found to be similar for both swirl levels, the starting location of the flame showed a vast difference in how the flame progressed. In general, the flame kernel was formed two crank-angle degrees after spark timing for the high swirl level, which was four crank-angle degrees earlier than that of the low swirl case. For the low swirl flow, the early combustion showed more cycle-to-cycle variation in terms of both the flame size and centroid location. It was quantitatively shown that increasing the swirl ratio from 0.55 to 5.68 could reduce the cycle-to-cycle variation of the early flame structure, resulting in about three to four crank-angle degrees advance of the peak pressure location and a 1% improvement for the coefficient of variation (COV) of the indicated mean effective pressure (IMEP). [DOI: 10.1115/1.4027256]

Introduction

Recently, vehicles equipped with spark-ignition direct-injection (SIDI) engines have demonstrated great potential in improved combustion efficiency and lower pollutant emissions [1]. However, elucidated by the method of how fuel is directly injected and immediately interacts with the incoming air through the intake ports, the combustion process strongly depends on the fuel-air mixture formation inside the combustion cylinder. It is well known that combustion does not behave in the same manner for consecutive engine cycles, even under the exact same engine condition due to the turbulent nature of the in-cylinder air motion [2,3]. As a result, the in-cylinder pressure curve varies quite substantially over many engine cycles. However, excessive variations of the engine output in terms of the indicated mean effective pressure (IMEP) not only reduces the engine power, but also increases the fluctuations of engine torque and combustion stability, degrading the drivability and controllability of vehicle. In addition, the slow combustion cycles could result in partial or unstable combustion, which increase the hydrocarbon emission and fuel consumption.

The reasons for the combustion variations have been well documented [1]. One of them is the variation of the fuel-air mixture formation from cycle to cycle in the cylinder and, more importantly, in the vicinity of the spark plug prior to the ignition process [4–6]. Subsequently, the variability in early flame development could degrade the combustion quality. It is because small differences of the early flame development could generate very different in-cylinder combustion pressure characteristics upon which the engine power output was based. Therefore, it is important to understand how the flame is initiated as the combustion starts under realistic operating conditions in an engine.

It is widely recognized that taking combustion images inside an engine with optical access to its combustion chamber is a powerful method to investigate the combustion quality, particularly in the early flame development stage where the use of a pressure-sensor may not provide reliable combustion data. Thanks to the recent advances in high speed imaging hardware and advanced processing algorithms, researchers are able to determine more precisely the key characteristics such as the flame front development, flame structure, propagation speed, and cycle-to-cycle variations of combustion inside a real engine [7–12]. For example, Aleiferis et al. [13] investigated the early flame development in a lean-burn SIDI engine with an optical access to its combustion chamber to

[1]Corresponding author.

Contributed by the Combustion and Fuels Committee of ASME for publication in the Journal of Engineering for Gas Turbines and Power. Manuscript received February 13, 2014; final manuscript received February 21, 2014; published online May 2, 2014. Editor: David Wisler.

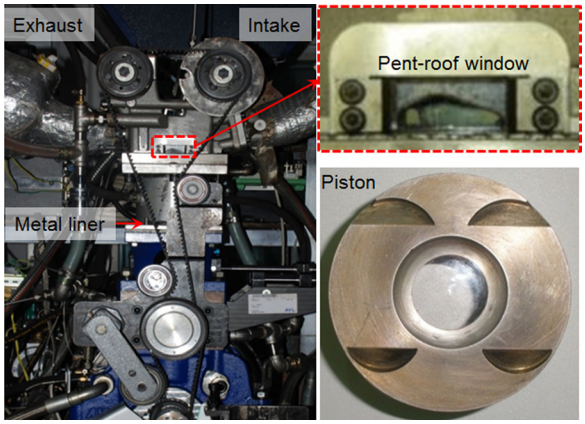

Fig. 1 Optical engine with a metal liner, pent-roof window, and upper piston with a quartz insert

Table 1 Engine parameters and operating conditions

Parameter	Value
Bore	86 mm
Stroke	94.6 mm
Connecting rod	160 mm
Clearance volume	54.95 cm^3
Displacement	549.51 cm^3
Compression ratio	11.0:1
Intake valve open (IVO)	366 deg BTDCF
Intake valve close (IVC)	114 deg BTDCF
Exhaust valve open (EVO)	131 deg ATDCF
Exhaust valve close (EVC)	372 deg ATDCF
Engine speed	800 rpm
Fuel injection pressure	10 MPa
Injection duration	915 μs
Fuel mass/cycle	10.7 mg
Manifold absolute pressure (MAP)	40 kPa
Air/fuel ratio	14.7
Start of injection (SOI)	300 deg BTDC
Spark timing	15 deg BTDC

study the cycle-to-cycle variability of engine combustion. They demonstrated that the initial flame kernel formation played a vital role for the later progress in combustion. Similarly, Keck et al. [14] demonstrated that the cyclic variations in the early flame location and growth rate were the major causes for the in-cylinder pressure cycle-to-cycle variation.

The charge motion of the fuel-mixture formation has been extensively studied as a way to enhance the combustion efficiency in internal combustion engines. In particular, a swirl control valve (SCV) can be adopted to enhance the fuel air mixing inside the combustion cylinder. For example, an SCV in a four-valve (two intake valves, two exhaust valves) SIDI engine has been demonstrated to accelerate the combustion process at idle and low-speed operating conditions [15,16]. Since each intake valve has its own intake port, the SCV is located in one of the two intake ports. Strong swirl motion can be introduced into the cylinder by closing the SCV. Li et al. [17] utilized laser Doppler anemometry to study the flow characteristics under both the SCV open and close conditions. When the SCV was deactivated (valve open), large-scale flow structures inside the cylinder were found, which were mainly composed of a tumble motion. These structures were distorted and broken up during the later stage of the compression stroke. Thus, small scale eddy and turbulence structures increased near the end of the compression stroke due to the strong breakup in the tumble direction. When the SCV was activated (valve close), the swirl motion was much stronger and was sustained longer until the end of the compression stroke. Frieden and Sick [18] demonstrated

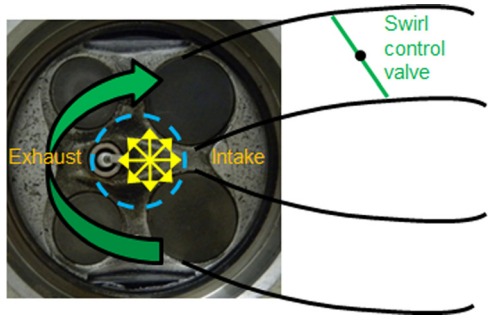

Fig. 2 Bottom view of the cylinder head; the dashed line shows the field of view (with a diameter of 26 mm)

that a high swirl flow produced a less homogeneous charge motion than the low swirl flow at spark timing and the high swirl significantly increased the combustion speed. Mittal and Schock [19] used the molecular tagging velocimetry measurement diagnostic to study the influence of the charge motion control valve (CMCV) on the cycle-to-cycle variations on in-cylinder flow. They found that the charge motion control had a profound effect on controlling the variations during intake and early compression, but the influence was progressively reduced during the late compression. Thus, they assumed that the CMCV improved the fuel-air mixing more than the combustion speed.

In summary, previous studies showed that the SCV can improve the engine performance through two methods: (1) enhancing the fuel-air mixing, fuel transport, fuel distribution, and evaporation, and (2) significantly increasing the flame speed. However, the study of the early flame development and its variation are still limited. Therefore, the objective of this paper is to experimentally investigate the early flame development at the engine idle condition inside the cylinder of a SIDI engine under different intake swirl flow levels. Simultaneous high speed combustion imaging and in-cylinder pressure recording under (1) low swirl (SCV open, swirl ratio of 0.55), and (2) high swirl (SCV closed, swirl ratio of 5.68) conditions are performed. The early flame formation and the variations are compared for these two swirl flow conditions. The current investigation also focuses on the cycle-to-cycle analysis of individual flames, including the flame size, location, and spatial characteristics on consecutive engine cycles.

Experimental Apparatus and Procedure

Optical Engine Assembly and Combustion Measurements. A single-cylinder four-stroke optical SIDI engine was used in this study. The engine was equipped with a four-valve pent-roof cylinder head which was based on a configuration of a General Motors prototype four-cylinder 2.0 L engine. The optical access to its cylinder was achieved through two locations: (1) two pent-roof windows, which allow for the view through the engine head clearance volume, and (2) a quartz-insert piston with the Bowditch extended piston design. The pent-roof windows also facilitated a close view of the flow field in the vicinity of the spark plug (shown) and injector tip (not shown). The four semicircular grooves were designed to avoid any unnecessary contact between the intake/exhaust valves to the piston top. A picture of this research engine is depicted in Fig. 1. The specific engine parameters and their values are tabulated in Table 1. The spark plug and a specially designed eight-hole SIDI fuel injector were centrally mounted on the cylinder head, which were in close proximity of each other. A piezoelectric pressure transducer (Kistler 6125A) was installed for acquiring the in-cylinder pressure measurements. The engine head configuration is shown in Fig. 2.

As previously mentioned, the SCV was installed in one of the intake air ports in order to enhance the clockwise swirl air motion entering the cylinder. High swirl was introduced into the cylinder

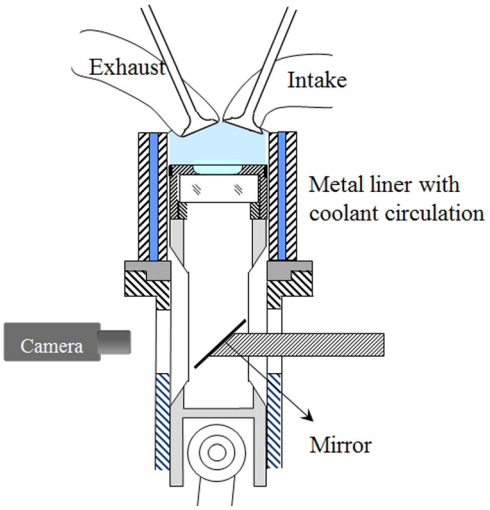

Fig. 3 Experimental setup of the imaging diagnostics

by fully closing the swirl control valve, as illustrated in Fig. 2. The dashed line shows the field of view of the combustion chamber through the quartz piston insert (with a diameter of 26 mm). For the tests in this study, a metal liner with a water coolant system was used instead of a quartz cylinder liner. If full optical access is necessary to image the fuel injection inside the cylinder, the metal liner can be replaced with the quartz liner.

The engine was motored by the AVL AC dynamometer (AVL List GmbH, Graz, Austria) at 800 rpm in this test. Since the engine only consisted of one cylinder, the AVL customized balance system was used to guarantee the engine operating at the lowest vibration level. A throttle valve was used to control the intake manifold absolute pressure (MAP) regulated at 40 kPa. A high-speed camera (Vision Research, Phantom V7.3) aiming into a 45 deg mirror located inside the elongated piston was used to record the luminosity of direct combustion. The experimental setup is shown in Fig. 3. Both the temporal and spatial evolution of the combustion process was studied by recording 91 images (400 × 400 pixels) per engine cycle at 9600 Hz (two images per crank angle degree). At the same time, the in-cylinder pressure was measured with a resolution of 0.1 crank angle degrees (CAD) simultaneously. The combustion images and their corresponding in-cylinder pressure measurements from 125 consecutive cycles were recorded for one test. Then, due to the limited memory storage of the camera and the dirty engine, the engine was cleaned and the recorded combustion images were transferred to the computer hard drive before the next test. Afterwards, the same test was performed again. In this way, the combustion images corresponding to a total of 250 engine cycles, with 91 images per cycle, together with the in-cylinder pressure, were obtained for every test condition.

In order to examine the effect of the SCV on flame initiation, the tests were performed under the following two intake air conditions: (1) high swirl, which was achieved through fully blocking

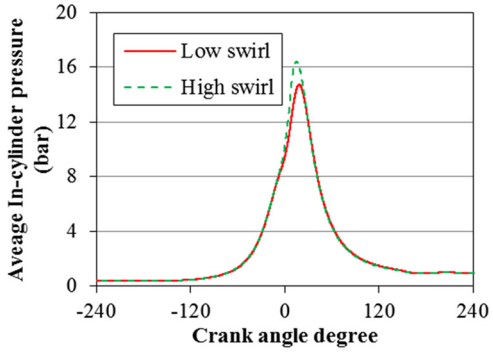

Fig. 5 Average in-cylinder pressure curves for the low and high swirl levels

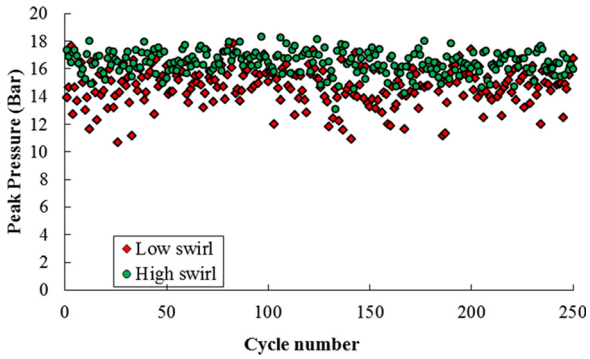

Fig. 6 Peak pressure of 250 consecutive combustion cycles

one of the intake ports; and (2) low swirl, which was realized by fully opening both intake ports. The in-cylinder pressure data was used for the calculations of the engine IMEP. Then the correlation between the IMEP and peak pressure parameters was correlated with the characteristics of the combustion images. The cycle-to-cycle variation for both engine swirl flow conditions were compared and analyzed.

Processing of Combustion Images and Data Extraction. To obtain quantitative information from the combustion process, the combustion images were processed in order to determine the structure and other characteristics of the flame such as the flame boundary, size, centroid location, and its propagation (see Fig. 4). Even though the recorded combustion image was the 2D projection image of a 3D flame, it still provided important and useful information such as the flame location and flame size. The raw flame images were processed in the following manner. First, a binarized combustion image was created from the raw 14-bit grayscale combustion image. More specifically, since the background noise intensity was smaller than five counts, a user-defined threshold of 10 counts (this value was maintained for other conditions)

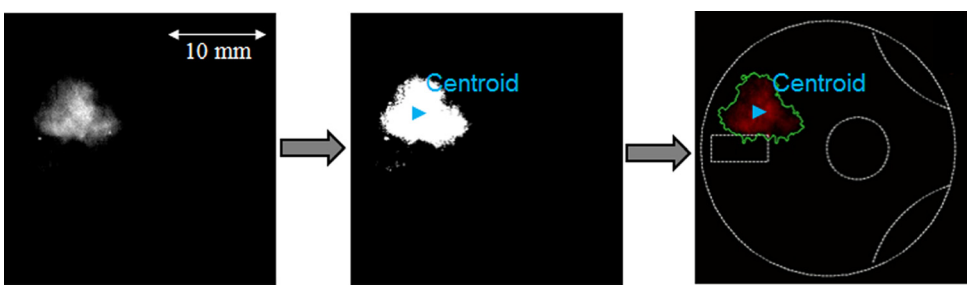

Fig. 4 Processing method for extracting the boundary centroid and locations of flame images

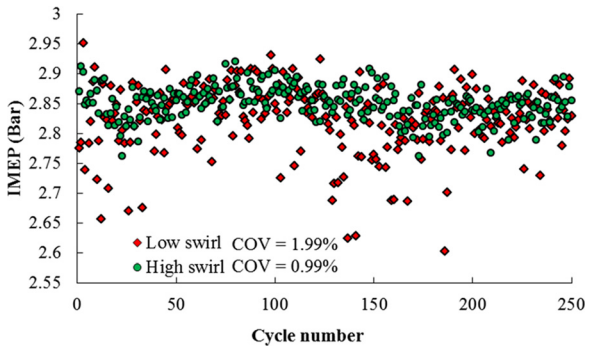

Fig. 7 IMEP of 250 consecutive combustion cycles

was set to identify the flame presence area. In other words, the image pixels with an intensity larger than 10 were set to be a value of 1 and the other pixels were set to be 0. Then the flame boundary was identified to be the separating line of the values of 0 and 1 in the binarized image. Afterwards, the centroid location of the binarized flame image was extracted. In this way, the early flame location was represented using a single point. Finally, the combustion image was displayed in false-color mode using a built-in "hot colormap" script in the MATLAB library. The final image was overlaid with the features of the cylinder such as the valves, injector tip, and spark plug to illustrate the position and size of the flame relative to the combustion chamber.

Results and Discussions

Prior to examining the characteristics of early flame development on a cycle-to-cycle basis, it is important to first reveal how swirl flow might influence the engine output on a cycle-ensemble perspective. Figure 5 shows the average pressure curves in the cylinder over the combustion cycle. They represent an average of 250 combustion cycles for both swirl levels. It is clearly seen that the high swirl level provided a slightly faster combustion. The peak location of the in-cylinder pressure was 18.5 crank angle degrees (CAD) after top dead center (TDC) at low swirl and 14.8 CAD after TDC at high swirl level. The average value of the peak cylinder pressure also showed comparable differences between the two swirl levels. The peak in-cylinder peak of the high swirl level reached 16.4 bar, whereas the peak pressure for the low swirl level only peaked with a value of 14.8 bar. There was a difference of about 10% between them. The corresponding peak pressure and IMEP (gross quantity) of the 250 consecutive cycles are displayed in Figs. 6 and 7, respectively. While the data points were randomly dispersed, the overall scattering of the peak values confirms that among these 250 cycles, the higher swirl level produced both a higher combustion peak pressure with a larger mean IMEP than the lower swirl level. As expected, the higher swirl level resulted in a higher average IMEP of 2.85 bar and the corresponding coefficient of variation (COV) of the IMEP was only 0.99%. On the contrary, the mean IMEP for the low swirl condition was 2.83 bar and the 250 cycles scattered much more with a COV of IMEP 1.99%, which was almost twice that of the high swirl condition.

Next, the focus is directed towards the examination of the early flame development and their variations over consecutive combustion events on a cycle-to-cycle basis. Figures 8 and 9 show the progression of the early flame development at both swirl levels. Four cycles from each swirl level have been selected to represent the typical observations found for these in-cylinder flow conditions. The first image on the left was selected when the flame was just initiated and its area reached a size of nearly 1 mm^2. The rest

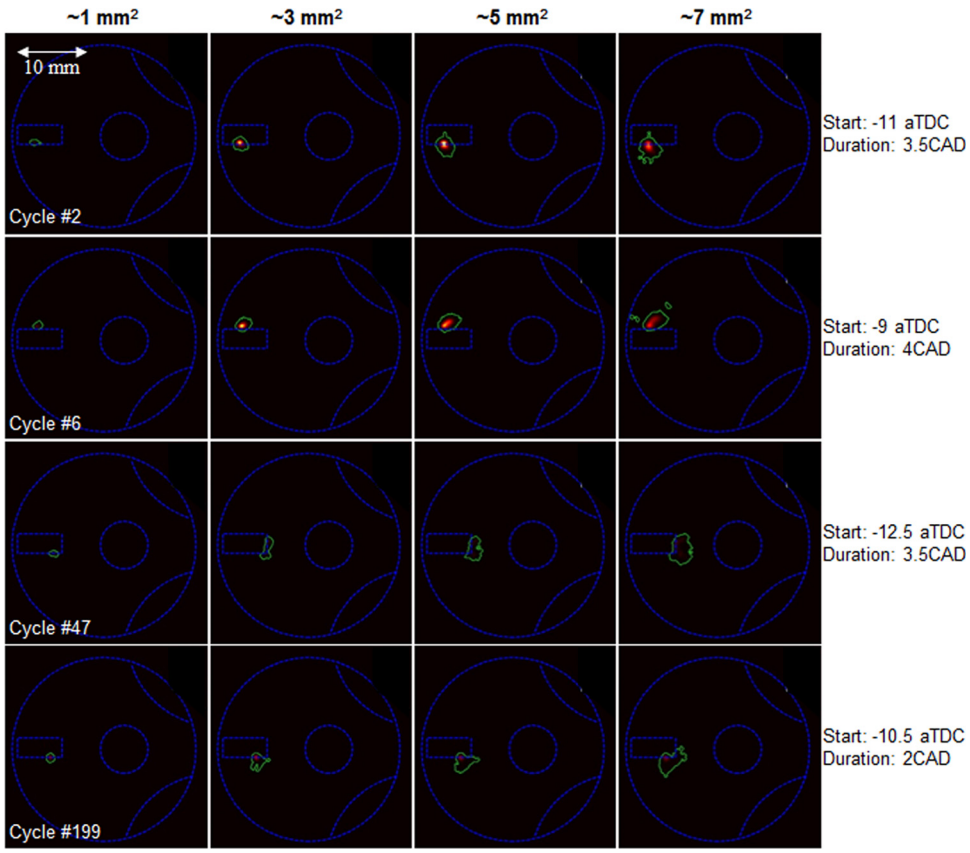

Fig. 8 Four representative combustion cycles of early flame development recorded from the low swirl level

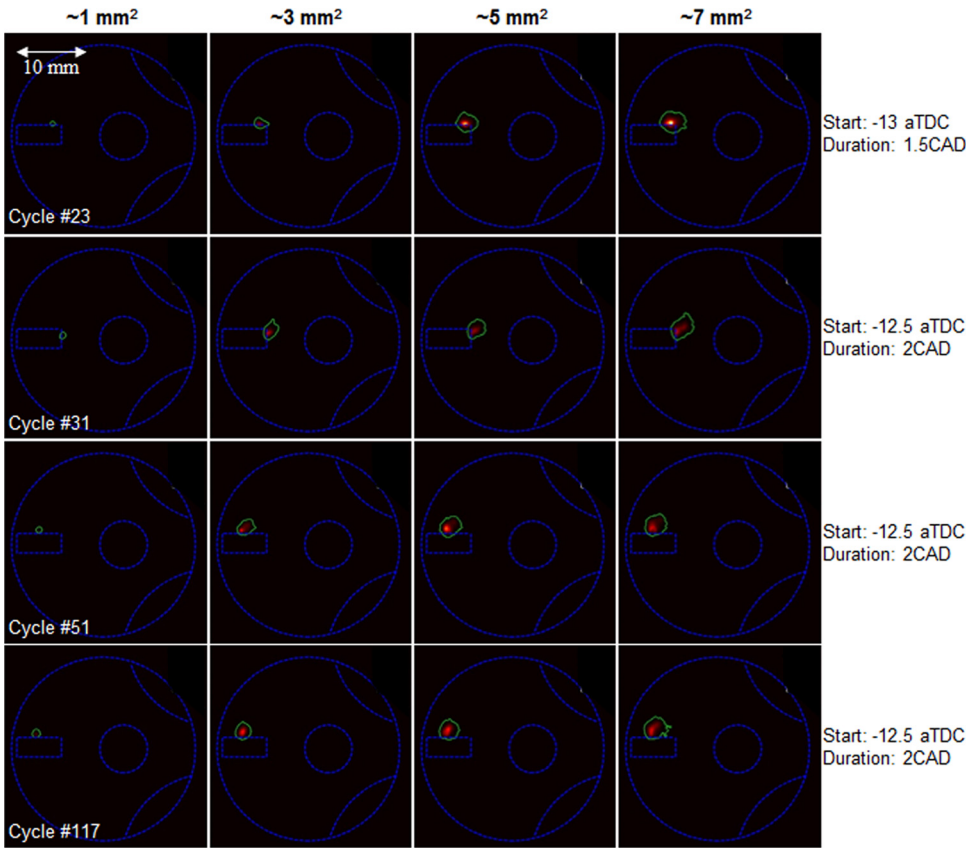

Fig. 9 Four representative combustion cycles of early flame development recorded from the high swirl level

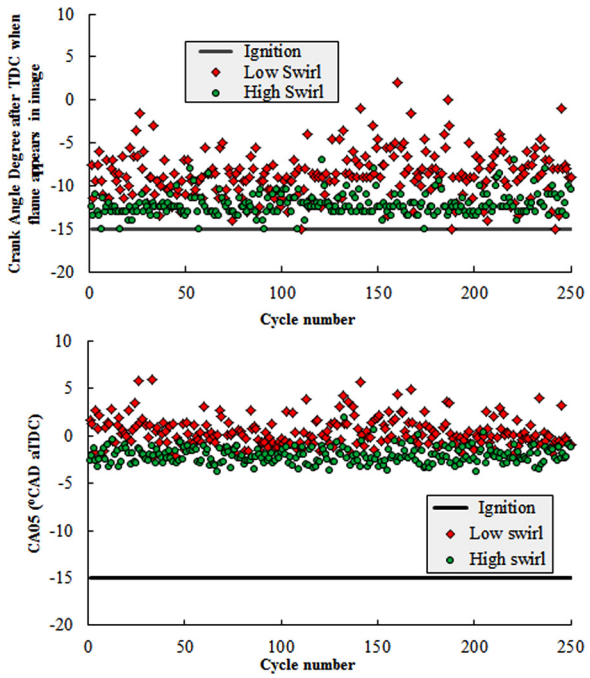

Fig. 10 Starting time variation of flame kernel formation (top), and CA05 location variation (bottom) over 250 combustion cycles

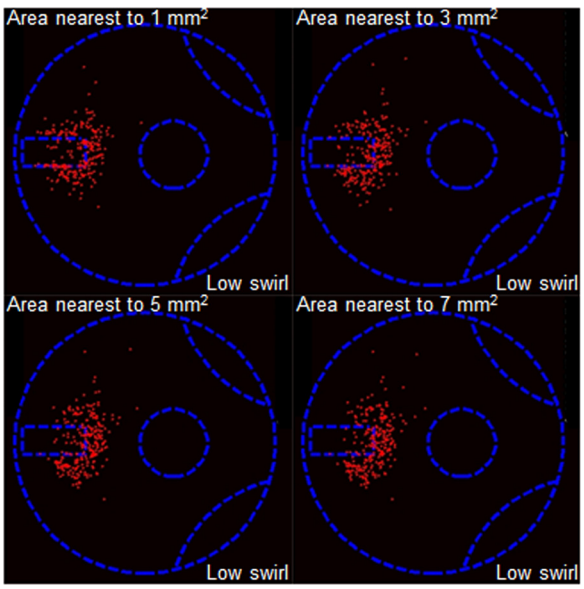

Fig. 11 Cycle-to-cycle variation of centroid locations under low swirl conditions, corresponding to flame areas of 1 mm², 3 mm², 5 mm², and 7 mm², respectively

of the images corresponded to the flame size reaching approximately 3 mm², 5 mm², and 7 mm² of the propagation of the same flame development.

For the initial flame combustion images of the low swirl level depicted in Fig. 8, the early flame kernel started in close proximity to the spark plug, but the starting locations surrounding it varied considerably. For example, it can be seen that the flame for cycle no. 2 started on the right side of the plug, while the flame started on the left side for cycle no. 6. The flame kernel also started at

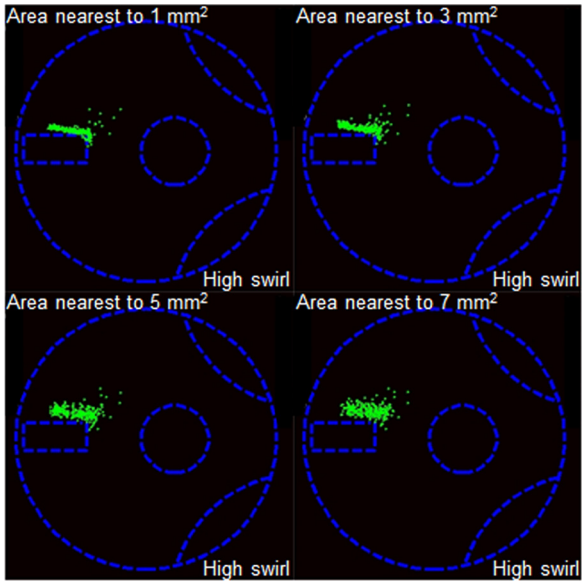

Fig. 12 Cycle-to-cycle variation of centroid locations under high swirl conditions, corresponding to flame areas of 1 mm², 3 mm², 5 mm², and 7 mm², respectively

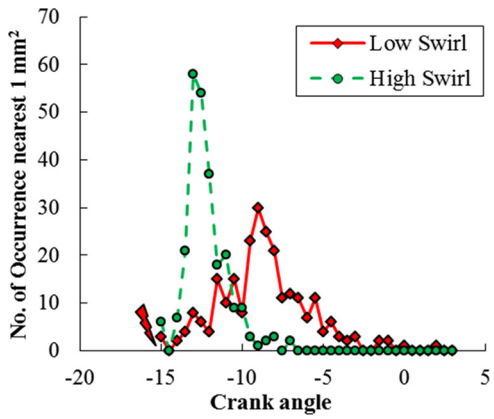

Fig. 13 Distribution of the number of flame cycles reaching 1 mm² under two swirl levels

different times: at 11 CAD before TDC (0 CAD) for cycle no. 2 and at 9 CAD before TDC for cycle no. 6. In general, it took about 3.5 to 4 CAD for the flame to progress from 1 mm² to 7 mm². However, take cycle no. 199 (bottom one on Fig. 8) as an illustration. The flame started at 10.5 CAD before TDC and it only took 2 CAD to grow to a size of 7 mm². The initial flame propagation for this cycle was almost twice as fast as the other three cycles shown. The flame in cycle no. 47 started at the earliest among the four, at 12.5 CAD before TDC, and the starting was at the tip of the plug instead of on either side. The natural flame luminosity for all cycles also varied greatly among these four cycles. As expected, all four flames propagated in a comparable fashion with a similar geometrical pattern. However, the flames of cycle nos. 2 and 6 had a higher natural luminosity than the other two cycles displayed. It is worth mentioning that while the actual color of the flame was mostly in pale blue, the images displayed in Figs. 8 and 9 had been reprocessed with a user-defined pseudo coloring scheme, as shown with a combination of red, orange, and yellow colors.

Reviewing the initial flame combustion images for the high swirl level, one can immediately identify that the cycle-to-cycle variations are considerably less than that of the low swirl levels.

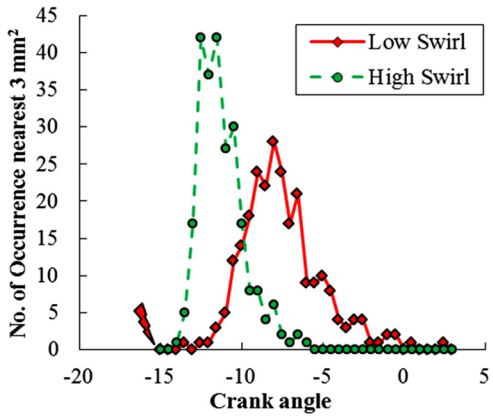

Fig. 14 Distribution of the number of flame cycles reaching 3 mm² under two swirl levels

Based on the metrics of the initial starting location, starting time, pseudo color, and pattern of the initial flame structure, it can be seen that the four cycles showed very consistent behavior. The flame started mostly at the left side of the spark plug. The starting time was around 13 CAD before TDC and it took only about 2 CAD for the flame to grow to nearly 7 mm². For example, the flame in cycle no. 23 started at the earliest moment and it only took 1.5 CAD to reach a size of 7 mm². Overall, the flame propagation speed for the high swirl level was almost twice that in the low swirl level.

Figure 10 depicts the starting time variation of the initial flame and the CA05 variation at both swirl levels (when the flame area reached 1 mm²). The fuel mixture was ignited at 15 CAD before TDC. It can be realized that for several cycles, flames started immediately as soon as ignition was initiated. For the high swirl level, most flames were found to start developing between 12 and 13 CAD before TDC and only a few cycles in which the flame started as late as around 6 CAD before TDC. On the contrary, for the low swirl level, the starting time of the flame scattered in a much wider manner. Besides a few cycles which started at 15 CAD before TDC, the majority of the cycles started between 12 and 8 CAD before TDC. For several outlier cycles, the flame was even initiated around or beyond TDC at 2 CAD when the piston started to move downward. A very similar observation could be found in the CA05 distribution in Fig. 10, suggesting the correlation between the flame image and in-cylinder pressure measurements. This is intuitively reasonable that the early flame appearance led to early CA05. In addition, the stable early flame appearance distribution results in a stable CA05 distribution for the high swirl case. Overall, for the 250 cycles under a low swirl level, the average starting time was 8.6 CAD before TDC with a COV of 31.6%, while for the high swirl level, the flame started much earlier at 12.2 CAD before TDC with a COV of 10.7%. Therefore, based upon this set of test results, it can be concluded that a higher swirl level inside the cylinder promoted the ignition process with a faster and lower cycle-to-cycle variation of flame initiation after ignition was commanded.

Further illustrations of the geometrical characteristics of the early flame development for all 250 cycles, from the beginning of the flame kernel until the flame reached 7 mm², are depicted in both Figs. 11 and 12. Note that the limit of 7 mm² was selected so that the entire flame boundary could be clearly contained within the visible limitation of the quartz piston insert. If any part of the flame extended beyond the boundary of the circular edge of the quartz-piston insert, the outside portion of the flame would not be accounted for. Thus the determination of the flame centroid would be not accurate.

In these two figures, the flame centroid locations of all 250 cycles were overlaid on the cylinder head configuration. The flame centroid is a good indication of the spatial scattering of the

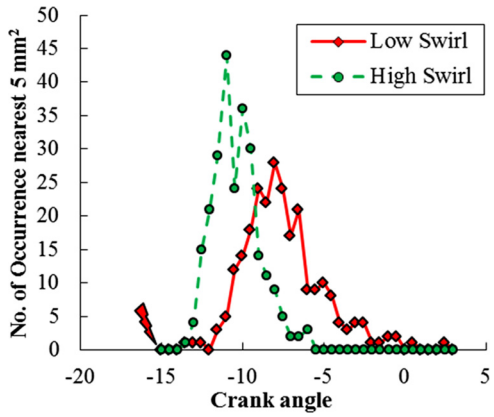

Fig. 15 Distribution of the number of flame cycles reaching 5 mm^2 under two swirl levels

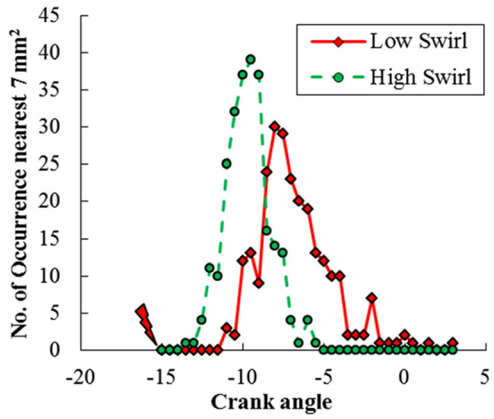

Fig. 16 Distribution of the number of flame cycles reaching 7 mm^2 under two swirl levels

flames. Comparing the locations of the centroid of the initial flame (1 mm^2 flame area), one can realize that a larger scattering of the centroid locations under a low swirl level was present. As the flame continued to grow to 7 mm^2, their positions were rather consistent surrounding the spark plug. For the high swirl level, all of the flames started at the upper left side of the spark plug. The more directed and concentrated locations of the flame initiation could be due to the fact that the initial spark or flame kernel was stretched in that direction by the in-cylinder air motion. It is also worth noticing that once the flame started at a specific position, it continued to grow relative to that location. Once started, flames were unlikely to jump around the cylinder spatially at the early stage. This observation seems valid for both low and high swirl levels.

The following set of figures (see Figs. 13–16) illustrates the comparison of the distribution of the number of flame cycles reaching a specific flame size of 1 mm^2, 3 mm^2, 5 mm^2, and 7 mm^2 under both swirl ratios. Note that the ignition was set at 15 CAD before TDC. Two observations can be readily obtained: (1) the initial flame kernel started much sooner after the ignition under the high swirl level than under the low swirl level, and (2) the distribution of the number of flames for the high swirl level was much more uniform (in other words, narrower) than that of the low flow level for all four flame sizes. This indicates that the higher swirl flow promotes a faster flame combustion than the low swirl ratio.

It is evident that there was less variation of the flame kernel formation under the high swirl level. As illustrated in Fig. 13, for the high swirl level with a flame area reaching 1 mm^2, there were nearly 60 cycles which started at 12 CAD before TDC and almost

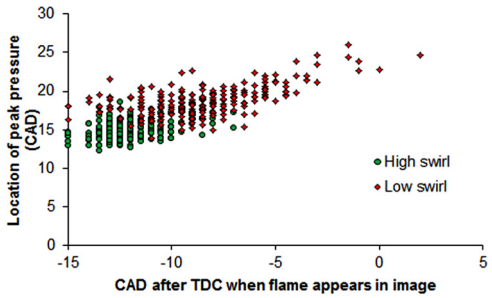

Fig. 17 The correlation between the early flame (1 mm^2) and peak pressure locations

all cycles started on or before 10 CAD before TDC. In contrary, for the low swirl level, only about one-third of the flames started on or before 10 CAD before TDC. Similar trends can be found for other flame sizes.

Lastly, the peak pressure locations (in CAD) are correlated with the initial flame locations (in CAD), as depicted in Fig. 17. First, a linear correlation is found for both swirl ratios, i.e., early flame kernel leads to early peak pressure. Second, it is evident that the high swirl flow accelerates the early flame propagation and results in an earlier peak pressure location than that of the low swirl flow ratio. To have an optimum engine output and efficiency, the location of the peak pressure should be between 13 deg CAD and 15 deg CAD ATDC. Therefore, as depicted in Fig. 17, a high swirl flow can advance the location of the peak pressure to around 15 deg CAD ATDC, which would improve the engine efficiency and output work.

Conclusions and Future Work

In this investigation, engine tests were performed to reveal the cycle-to-cycle variation of the early flame development of combustion in a single-cylinder spark-ignition direct-injection engine. The crank angle resolved combustion images inside the combustion chamber and in-cylinder pressure measurements of 250 consecutive cycles were simultaneously recorded for both intake air flow swirl levels (swirl ratio of 0.55 and 5.68). The following observations are found under the current engine test conditions:

(1) Flame initiation is strongly affected by the swirl flow levels inside the combustion chamber. Overall, the initial flame kernel appears about 4 CAD earlier than that of the low swirl case. In addition, the high swirl flow promotes the early flame kernel propagation speed to be roughly twice that for the low swirl case. The high swirl early flame locations are much more repeatable than that of the low swirl case.
(2) The analysis of the cycle-to-cycle variations of the flame characteristics reveals more details of how the early flame is developed and propagated.
(3) The high swirl level produces a lower variation in the early flame structure on a cycle-to-cycle basis, leading to higher combustion stability (1% improvement for the COV of the IMEP) and faster combustion. More specifically, the high swirl flow advances the location of the peak pressure to about 15 CAD ATDC, which would improve the engine output work and efficiency.

This investigation was performed when the piston quartz insert diameter was 26 mm. In order to ensure that the entire flame boundary was clearly contained within the visible limitation of the quartz piston insert, the maximum flame size was limited to only 7 mm^2 in this study. It was rather small compared to the actual bore of the piston, limiting the visible area of the combustion process and the accuracy of the data extraction. Since then, a new piston with a quartz insert with a diameter of 64 mm has been assembled in order to allow a much larger viewing area for

combustion visualization. Future work will also be focused on gathering additional combustion images to correlate the initial flame structure with the burn rate to understand the flame development at higher engine and load conditions. In addition, different fuels would affect the variation in the fuel mixture formation and combustion processes of fuel injected engines. Renewable fuels such as alcohol-based fuels will be investigated in the future for the understanding of early flame development.

Acknowledgment

This research is sponsored by General Motors R&D (USA) and the National Natural Science Foundation of China (NSFC) under Grant Nos. 51076093/E060702 and 51176115/E060404 and was carried out at the National Engineering Laboratory for Automotive Electronic Control Technology of the Shanghai Jiao Tong University. Additional funding support on this research to D.L.S. Hung has also been provided by the 2009 Program for New Century Excellent Talents in University by the Ministry of Education (MOE), China.

References

[1] Zhao, F., Lai, M. C., and Harrington, D. L., 1999, "Automotive Spark-Ignited Direct-Injection Gasoline Engines," Prog. Energy Combust. Sci., **25**(5), pp. 437–562.
[2] Chen, H., Reuss, D. L., Hung, D. L. S., and Sick, V., 2013, "A Practical Guide for Using Proper Orthogonal Decomposition in Engine Research," Int. J. Engine Res., **14**(4), pp. 307–319.
[3] Chen, H., Reuss, D. L., and Sick, V., 2012, "On the Use and Interpretation of Proper Orthogonal Decomposition of In-Cylinder Engine Flows," Meas. Sci. Technol., **23**(8), p. 085302.
[4] Peterson, B., Reuss, D. L., and Sick, V., 2011, "High-Speed Imaging Analysis of Misfires in a Spray-Guided Direct Injection Engine," Proc. Combust. Inst., **33**(2), pp. 3089–3096.
[5] Chen, H., Reuss, D., and Sick, V., 2011, "Analysis of Misfires in a Direct Injection Engine Using Proper Orthogonal Decomposition," Exp. Fluids, **51**(4), pp. 1139–1151.
[6] Peterson, B. and Sick, V., 2009, "Simultaneous Flow Field and Fuel Concentration Imaging at 4.8 kHz in an Operating Engine," Appl. Phys. B, **97**(4), pp. 887–895.
[7] Schiebl, R., Dreizler, A., and Maas, U., 1999, "Comparison of Different Ways for Image Post-Processing: Detection of Flame Fronts," SAE Technical Paper No. 1999-01-3651.
[8] Bates, S. C., 1989, "Flame Imaging Studies in a SI Four-Stroke IC Optical Engine," SAE Technical Paper No. 890154.
[9] Bates, S. C., 1989, "Cycle-by-Cycle Combustion Variation in a SI Four-Stroke Engine," SAE Technical Paper No. 892086.
[10] Aleiferis, P. G., Serras-Pereira, J., and Richardson, D., 2013, "Characterisation of Flame Development With Ethanol, Butanol, Iso-Octane, Gasoline and Methane in a Direct-Injection Spark-Ignition Engine," Fuel, **109**, pp. 256–278.
[11] Sick, V., Drake, M. C., and Fansler, T. D., 2010, "High-Speed Imaging for Direct-Injection Gasoline Engine Research and Development," Exp. Fluids, **49**(4), pp. 937–947.
[12] Sick, V., 2013, "High Speed Imaging in Fundamental and Applied Combustion Research," Proc. Combust. Inst., **34**(2), pp. 3509–3530.
[13] Aleiferis, P. G., Taylor, A. M. K. P., Ishii, K., and Urata, Y., 2004, "The Nature of Early Flame Development in a Lean-Burn Stratified-Charge Spark-Ignition Engine," Combust. Flame, **136**(3), pp. 283–302.
[14] Keck, J. C., Heywood, J. B., and Noske, G., 1987, "Early Flame Development and Burning Rates in Spark Ignition Engines and Their Cyclic Variability," SAE Technical Paper No. 870164.
[15] Endres, H., Schulte, H., and Krebs, R., 1990, "Combustion System Development Trends for Multi-Valve Gasoline Engines," SAE Technical Paper No. 900652.
[16] Leo, M., Friedrich, Q., and Gunter, F., 1990, "Development of Low Emission High Performance Four Valve Engines," SAE Technical Paper No. 900027.
[17] Li, Y., Liu, S., Shi, S.-X., and Xu, Z., 2000, "Effect of the Swirl Control Valve on the In-Cylinder Air Motion in a Four-Valve SI Engine," SAE Technical Paper No. 2000-01-2058.
[18] Frieden, D. and Sick, V., 2003, "Investigation of the Fuel Injection, Mixing and Combustion Processes in an SIDI Engine Using Quasi-3D LIF Imaging," SAE Technical Paper No. 2003-01-0068.
[19] Mittal, M. and Schock, H. J., 2010, "A Study of Cycle-to-Cycle Variations and the Influence of Charge Motion Control on In-Cylinder Flow in an IC Engine," ASME J. Fluids Eng., **132**(5), p. 051107.